MALAYSIAN JOURNAL OF MICROSCOPY

Journal homepage: https://malaysianjournalofmicroscopy.org

RESEARCH ARTICLE

COMPARATIVE HALF-CELL ANALYSIS OF SULFUR-, NITROGEN-, AND FLUORINE-DOPED REDUCED GRAPHENE OXIDE ANODES

Mohamad Taufiq Mohamad Alias[1], Nur Ezyanie Safie[1,*], Siti 'Aishah Azman[1], Nurul Syuhada Mohd Shari[1], Najmiah Radiah Mohamad[2], Eleen Dayana Mohamed Isa[3], Mohd Asyadi Azam[4]

[1]Fakulti Teknologi dan Kejuruteraan Elektrik, Universiti Teknikal Malaysia Melaka, Malaysia.
[2]Fakulti Teknologi dan Kejuruteraan Elektronik dan Komputer, Universiti Teknikal Malaysia Melaka, Malaysia.
[3]Malaysia-Japan International Institute of Technology, Universiti Teknologi Malaysia, Malaysia.
[4]Fakulti Teknologi dan Kejuruteraan Industri dan Pembuatan, Universiti Teknikal Malaysia Melaka, Malaysia.

Abstract. Advanced lithium iron phosphate battery systems demand anode materials with higher capacity, better rate capability, and stronger structural stability than conventional graphite. This study investigates the electrochemical performance of functionalized reduced graphene oxide (rGO) as a potential anode material, focusing on sulfur (S), nitrogen (N), and fluorine (F) heteroatom doping. The materials were synthesized through controlled hydrothermal and thermal treatment methods and characterized using X-ray diffraction (XRD), field emission scanning electron microscopy (FESEM), and energy-dispersive X-ray (EDX) spectroscopy. Structural analysis showed that sulfur doping increased interlayer spacing and introduced more active defect sites, while nitrogen and fluorine doping enhanced graphitic alignment, as indicated by a sharper (002) peak near 26°, which corresponds to reduced interlayer spacing. Electrochemical properties were evaluated using cyclic voltammetry (CV) within a potential range of 0.01–3.0 V (vs. Li/Li^+). Among all samples, sulfur-doped rGO exhibited the strongest electrochemical performance, with the largest CV curve area and an apparent capacitance of 492.32 F g^{-1}, corresponding to a specific capacity of 408.90 mAh g^{-1}. Pristine rGO achieved 417.66 F g^{-1} (346.89 mAh g^{-1}), whereas nitrogen-doped and fluorine-doped samples showed lower values of 278.39 F g^{-1} (231.21 mAh g^{-1}) and 223.07 F g^{-1} (185.27 mAh g^{-1}), respectively. The results indicate that charge storage is mainly governed by pseudocapacitive surface reactions rather than bulk intercalation. Overall, sulfur-doped rGO demonstrated superior charge storage capability, highlighting its potential as an advanced anode material for next-generation $LiFePO_4$-based lithium-ion batteries.

Keywords: Functionalized graphene, reduced graphene oxide, graphene anode, anode material, LFP battery.

Article Info

Received 18 January 2026
Accepted 13 May 2026
Published 8 June 2026

***Corresponding author: ezyanie@utem.edu.my**

ISSN: 1823-7010, eISSN: 2600-7444

1. INTRODUCTION

The rapid expansion of electric vehicles, renewable energy systems, and portable electronic devices has significantly increased the global demand for high-performance lithium-ion batteries (LIBs) [1,2]. Key requirements for next-generation LIBs include high energy density, long cycle life, and excellent rate capability. However, conventional graphite anodes, despite their commercial maturity, suffer from limited theoretical capacity (372 mAh g^{-1}) and moderate rate performance, which restrict further improvements in overall battery performance [3]. To overcome these limitations, extensive research has focused on advanced carbon-based materials. Among them, reduced graphene oxide (rGO) has attracted considerable attention due to its high electrical conductivity, large specific surface area, and tunable surface chemistry [4,5]. The two-dimensional layered structure of rGO facilitates efficient electron transport and short lithium-ion diffusion pathways, making it a promising candidate for high-performance anode applications.

Various strategies have been explored to enhance the electrochemical properties of rGO, including composite formation with metal oxides and structural engineering approaches [6-8]. Although such hybrid systems often exhibit improved capacity and rate performance, their synthesis procedures can be relatively complex and may involve structural instability during repeated cycling due to volumetric changes of active components. Heteroatom doping has emerged as a simpler and more controllable method to tailor the physicochemical and electrochemical characteristics of graphene-based materials [4]. Incorporation of heteroatoms such as nitrogen, sulfur, and fluorine can modify the electronic structure, introduce defect sites, and alter interlayer spacing, thereby influencing lithium storage behavior and charge transfer kinetics. Nitrogen doping generally enhances electrical conductivity and creates electrochemically active sites, while sulfur doping can introduce redox-active functionalities and promote surface-dominated charge storage.

Fluorine incorporation, on the other hand, is often associated with improved structural stability and interfacial properties, although excessive fluorination may affect electronic conductivity [9]. Mechanistically, the incorporation of these heteroatoms alters the physicochemical landscape of graphene in distinct ways. Nitrogen doping shifts the Fermi level and increases localized electron density, thereby enhancing the Li^+ adsorption energy, particularly at pyridinic and pyrrolic active sites. Sulfur, possessing a larger atomic radius than carbon, physically expands the graphitic interlayer spacing, which lowers the energy barrier for lithium-ion diffusion pathways while creating distinct charge distribution imbalances that serve as redox-active sites. Conversely, the high electronegativity of fluorine induces strong localized C–F dipole moments that can firmly anchor Li^+ and stabilize the solid-electrolyte interphase, though excessive fluorination risks disrupting the delocalized sp^2 network and impeding bulk electronic conductivity.

Recent studies on heteroatom-modified graphene materials have demonstrated promising electrochemical performance and improved structural durability in lithium-ion systems [10-13]. However, evaluating the true comparative advantages of these dopants is challenging because existing literature largely investigates them in isolation under vastly different synthesis parameters. For example, independent studies show that hydrothermal nitrogen doping enhances planar conductivity and thermal fluorine doping improves interfacial stability, the use of different precursors, temperatures, and reduction times in these separate works obscures their relative electrochemical contributions. Without a baseline comparison under controlled, comparable synthesis conditions, it is difficult to determine whether variations in capacity and stability are driven by the specific heteroatom itself or by the distinct thermal and chemical environments used during its synthesis. Nevertheless, systematic comparisons between different dopants synthesized under comparable conditions remain limited. In particular, the relative influence of sulfur, nitrogen, and fluorine incorporation on crystallinity, defect chemistry, and electrochemical response requires further clarification.

While prior comparative studies often focus on co-doping synergies or rely on complex hierarchical composites, the specific research gap addressed here is the lack of an isolated, standardized

evaluation of individual S, N, and F dopants on graphene's structural evolution and half-cell electrochemical behavior. The novelty of this work lies in utilizing a unified, comparable synthetic framework to directly correlate each distinct heteroatom's structural impact, such as sulfur-induced active defect generation versus fluorine-induced planarization, to their resulting pseudocapacitive charge storage metrics, thereby establishing a fundamental baseline for rational anode design. Therefore, this study systematically investigates sulfur-, nitrogen-, and fluorine-functionalized rGO synthesized via scalable hydrothermal and thermal approaches as a preliminary screening study. Structural and morphological characteristics were examined using X-ray diffraction (XRD), field emission scanning electron microscopy (FESEM), and energy-dispersive X-ray spectroscopy (EDX). Electrochemical performance was evaluated through cyclic voltammetry in a half-cell configuration within the voltage window of 0.01–3.0 V (vs. Li/Li^+) to establish an initial baseline of their comparative charge storage behaviors prior to future extensive long-term cycling evaluations. This work provides comparative insights into the role of different heteroatom dopants in tailoring graphene-based anodes and highlights their potential application in lithium iron phosphate battery systems.

2. MATERIALS AND METHODS

All chemicals used in this study were of analytical grade. Sodium thiosulfate pentahydrate ($Na_2S_2O_3 \cdot 5H_2O$, ≥97 %), hydrochloric acid (HCl, reagent-grade), ethanol (≥99.5 %), and ammonia solution (25 wt.% NH_3 in H_2O) were sourced from Merck (Germany). The fluorine precursor, 1-butyl-3-methylimidazolium hexafluorophosphate (BMIM-PF_6, ≥97 %), was obtained from Sigma-Aldrich. Deionized (DI) water with resistivity >1 MΩ·cm was used throughout (Emsure® Type II), and reduced graphene oxide (rGO), used as the base material, was lab-grade and procured from IESB, Malaysia. All reagents were selected for their high purity to ensure consistency and reproducibility in material synthesis and characterization. All functionalized rGO materials were synthesized via hydrothermal methods, as schematically illustrated in Figure 1.

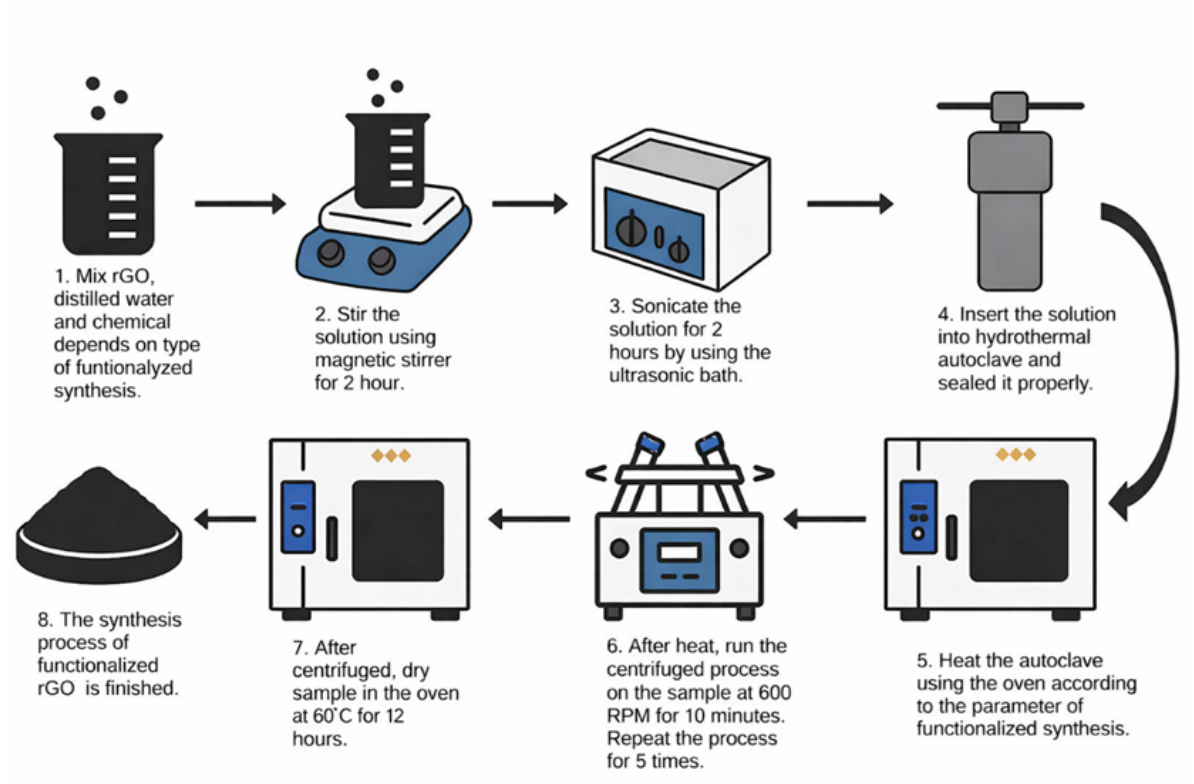

Figure 1: Simplified schematic of the hydrothermal synthesis process for functionalized reduced graphene oxide (rGO), including mixing, stirring, sonication, autoclave treatment, centrifugation, and drying. The procedure is tailored based on the dopant type (e.g., sulfur, nitrogen, fluorine)

While the core synthesis technique remained constant, the specific chemical agents introduced varied depending on the desired functional group (sulfur, nitrogen, or fluorine). The synthesis conditions and reagents for each functionalization pathway are described in subsections 2.1, 2.2, and 2.3.

2.1 Synthesis of Sulfur-Functionalized rGO (S-rGO)

To prepare sulfur-functionalized rGO, 5 mg of rGO was first dispersed in 5 mL of DI water under 30 minutes of ultrasonication to form a uniform colloidal suspension. Subsequently, 5 mL of 5 M sodium thiosulfate and 3 mL of 1 M hydrochloric acid were added dropwise while stirring. The mixture underwent further ultrasonication for 2 hours at 100 W and 40 kHz. This dispersion was then transferred into a 20 mL Teflon-lined stainless-steel autoclave and subjected to hydrothermal treatment at 180 °C for 12 hours. Upon cooling to room temperature, the solid product was isolated by centrifugation at 10,000 × g, rinsed with DI water and ethanol three times each, and dried in a vacuum oven at 80 °C for 24 hours. This process facilitated sulfur atom incorporation via chemical self-assembly mechanisms, enhancing electrical conductivity and functional surface sites.

2.2 Synthesis of Nitrogen-Functionalized rGO (N-rGO)

For nitrogen doping, 50 mg of rGO was dispersed in 50 mL of DI water and sonicated for 2 hours to form a homogeneous dispersion. Then, 20 mL of ammonia solution (25 wt.%) was slowly introduced under constant stirring. The resultant mixture was transferred to an autoclave and treated at 200 °C for 24 hours. This hydrothermal condition enabled simultaneous nitrogen incorporation and reduction of oxygen-containing groups on the graphene sheets. After natural cooling, the product was recovered via centrifugation, followed by thorough washing with DI water and ethanol, and vacuum-dried at 80 °C for 24 hours. The nitrogen dopant levels and bonding states were later confirmed using Energy-Dispersive X-ray Spectroscopy (EDX).

2.3 Synthesis of Fluorine-Functionalized rGO (F-rGO)

To synthesize fluorinated rGO, 50 mg of rGO was dispersed in 50 mL of DI water and ultrasonicated for 2 hours. Following this, 200 mg of BMIM-PF_6 was added and stirred for 1 hour to ensure sufficient interaction with rGO sheets. The suspension was transferred into a ceramic crucible and subjected to thermal treatment in a tube furnace at 200 °C for 24 hours under a nitrogen atmosphere. The fluorine atoms from the decomposition of BMIM-PF_6 were incorporated into the graphene lattice, enhancing its conductivity and chemical stability. The product was cooled, centrifuged, washed with DI water and ethanol, and vacuum-dried at 80 °C for 24 hours.

2.4 Electrode Fabrication

To evaluate the electrochemical performance, the synthesized functionalized rGO powders were fabricated into working electrodes. The electrode slurry was prepared by mixing the active material (functionalized rGO), a conductive additive (Super P), and a polymeric binder (polyvinylidene fluoride (PVDF)) in a weight ratio of 80:10:10. The mixture was dispersed in N-methyl-2-pyrrolidone (NMP) solvent and magnetically stirred to form homogeneous slurry. This slurry was then uniformly coated onto a copper foil current collector using a film coater. The coated electrodes were dried in a vacuum oven at 80 °C for 12 hours to remove residual solvent. Finally, the electrodes were punched into circular disks, with an average active material mass loading of approximately 1.0 mg cm^{-2} per electrode.

2.5 Material Characterization

The synthesized functionalized rGO materials (S-rGO, N-rGO, and F-rGO) were characterized structurally, morphologically, and electrochemically. X-ray diffraction (XRD) using a Rigaku MiniFlex

X-ray Diffractometer (Cu Kα, λ = 1.5406 Å) was employed to assess crystallinity and interlayer spacing, post-functionalization. The XRD patterns were recorded over a 2θ scan range of 10° to 60° with a step size of 0.01° and a scan rate of 1° min^{-1}. The degree of crystallinity (X_c) for each sample was quantitatively determined from the XRD data by peak deconvolution. The calculation was performed using the standard ratio of the integrated area of the crystalline peaks (A_c) to the total integrated area, which encompasses both the crystalline and amorphous (A_a) components, according to the following equation:

$$X_c(\%) = \frac{A_c}{A_a + A_c} \times 100 \quad (1)$$

Peak fitting and area integration were conducted using OriginPro software.

Morphological features were examined via Field Emission Scanning Electron Microscopy (FESEM, Hitachi Schottky FESEM SU5000), while elemental composition and dopant distribution were confirmed through Energy-Dispersive X-ray Spectroscopy (EDX). For electrochemical evaluation, cyclic voltammetry (CV) tests were performed in CR2032 coin cells using a Wonatech WMPG1000 potentiostat/galvanostat multichannel system. The CR2032 half-cells were assembled in an argon-filled glovebox. A polypropylene membrane was used as the separator. The electrolyte consisted of 2.0 M lithium hexafluorophosphate ($LiPF_6$) dissolved in a 1:1 volume ratio of ethylene carbonate (EC) and dimethyl carbonate (DMC). CV was conducted at 0.2 mV/s within 0.01–3.0 V (vs. Li/Li^+). The apparent specific capacitance (C, F g^{-1}) of the electrodes was calculated from the CV curves using the following standard equation:

$$C = \frac{\int IdV}{2\, m\, v\, \Delta V} \quad (2)$$

where ∫IdV is the integrated area of the cyclic voltammogram (A V), m is the mass of the active material in the electrode (g), ν is the scan rate (V s^{-1}), and ΔV is the operational potential window (V). These analyses provided comprehensive insight into the structural integrity and electrochemical performance of the functionalized rGO anodes in LFP battery systems. To ensure the reliability and reproducibility of the experimental results, all electrochemical measurements were performed on a minimum of three independent CR2032 coin cells for each material variant (pristine rGO, S-rGO, N-rGO, and F-rGO). The reported cyclic voltammetry (CV) curves represent the typical, stable electrochemical behavior observed across the replicates. Furthermore, the calculated apparent capacitance values and their corresponding specific capacities represent the average reproducible performance, with an estimated relative error of less than ± 3 % across the tested samples.

3. RESULTS AND DISCUSSION

3.1 Materials Properties

The X-ray diffraction (XRD) analysis as depicted in Figure 2 provides valuable insight into the crystalline and structural ordering of the graphene materials. Quantitative crystallinity analysis reveals distinct values across samples: rGO (33 %), F-rGO (47 %), N-rGO (54 %), and S-rGO (62 %). In the pristine reduced graphene oxide sample, the (002) diffraction peak appears broadly between 20° and 26°, indicating partial restoration of the sp^2-hybridized carbon framework but retaining significant disorder and layer misalignment. Similar results were reported, showing that thermally reduced GO retained disordered interlayer stacking with limited crystallite alignment [14]. Both nitrogen-doped (N-rGO) and fluorine-doped (F-rGO) samples exhibit a pronounced sharpening and increased intensity of the (002) peak at approximately 26°, signifying enhanced graphitic ordering and reduced interlayer spacings. The quantitative structural parameters extracted from the (002) diffraction peaks, including the precise 2θ positions, full width at half maximum (FWHM), calculated d-spacing, and degree of crystallinity for all samples, are summarized in Table 1. Such improvements in crystallinity are

consistent with established findings, where nitrogen incorporation facilitates planar sp^2 reinforcement, thereby enhancing electrical conductivity. For instance, Tasdemir et al. [6] reported enhanced conductivity and stacking order in N-doped graphene derived from thermal treatment.

The sulfur-doped sample presents a more intricate diffraction profile. While the broad (002) peak confirms the presence of the graphitic structure, additional sharp peaks are evident at 2θ = 23.1°, 25.8°, 26.7°, and 27.7°. These peaks are distinctly indexed to the [222], [026], [206] and [026] crystallographic planes of elemental orthorhombic sulfur (S_8), perfectly matching the standard reference data JCPDS card no. 08-0247. Literature reports have documented that sulfur doping can introduce ordered sulfur-rich phases, leading to supplementary diffraction features in XRD patterns. Notably, recent studies in catalytic contexts confirmed that, at moderate sulfur loadings, these secondary phases remain undetectable in XRD, implying sulfur exists either in amorphous form or as sub-nanocrystalline dispersed species where similar behavior was observed [15]. The appearance of extra peaks in our S-rGO sample thus likely reflects moderate sulfur aggregation, sufficient to create XRD-visible crystallinity without accumulating detectable large-scale sulfur crystals.

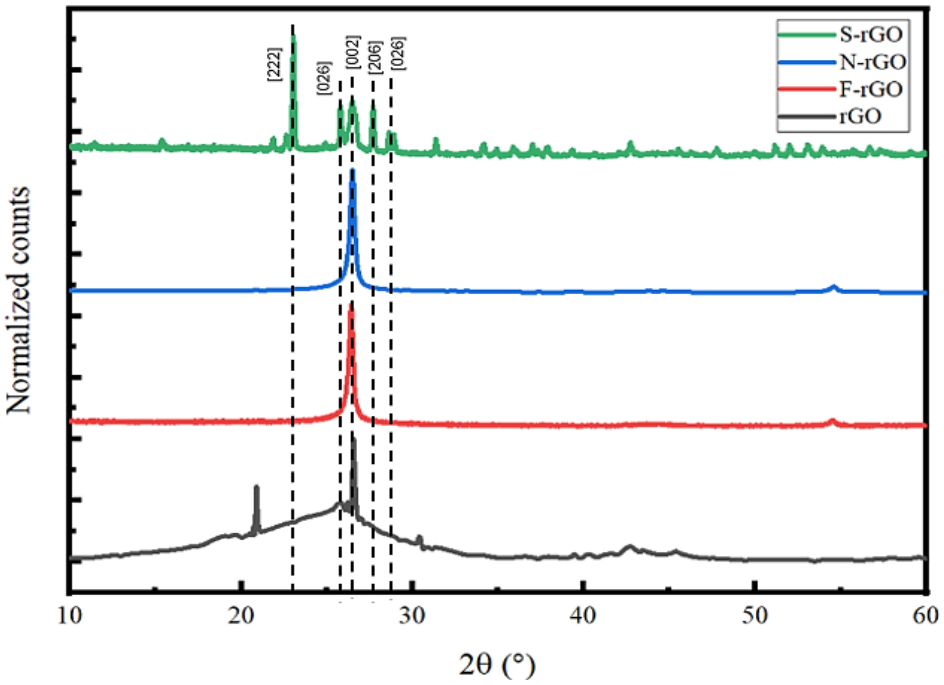

Figure 2: X-ray diffraction (XRD) patterns of pristine rGO and heteroatom-doped functionalized rGO samples (S-rGO, N-rGO, and F-rGO)

Table 1: Quantitative structural parameters of the synthesized functionalized rGO samples extracted from XRD analysis

Sample	2θ position (°) of [002] plane	FWHM	d-spacing (nm)	Crystallite size, L_c (nm)	Crystallinity (%)
rGO	24.4	7.65587	0.365	11.0838	33
F-rGO	26.4	0.40917	0.337	208.2075	47
N-rGO	26.5	0.44313	0.336	192.2906	54
S-rGO	26.5	0.48967	0.336	174.0146	62

Sulfur doping appears to disrupt lattice coherence but introduces functional groups that may enhance redox activity, whereas nitrogen and fluorine doping significantly improve graphitic crystallinity, which supports better electrical conductivity and structural stability [16]. The XRD patterns highlight how different dopants affect graphene ordering, with nitrogen and fluorine promoting

defect healing and planar alignment, while sulfur creates structural complexity that could enhance electrochemical reactivity but may also lead to reduced stability. Further studies correlating these structural features with electrochemical performance are necessary to determine whether ordered graphitic domains or dopant-induced functionalities offer greater benefits for anode applications.

The morphological and compositional features of reduced graphene oxide (rGO) and its heteroatom-doped derivatives were analyzed using Field Emission Scanning Electron Microscopy (FESEM) coupled with Energy-Dispersive X-ray Spectroscopy (EDX), as shown in Figures 3 and 4. FESEM imaging of pristine rGO (Figure 3(a)) reveals loosely stacked, wrinkled sheets typical of partially reduced graphene structures. This morphology offers a high surface area but also indicates structural disorder. Upon sulfur doping (S-rGO, Figure 3(b)), morphology transforms into denser aggregates with rougher textures, suggesting the formation of sulfur-functionalized domains or embedded sulfur clusters. EDX analysis confirms the successful incorporation of sulfur with a weight percentage of 6.4 percent and an atomic percentage of 2.6 percent (Figure 4(a)). Recent reports have indicated that sulfur species introduce active defect sites, which enhance lithium-ion transport and promote surface-controlled redox reactions, thereby improving the overall charge storage behavior as reported previously [10].

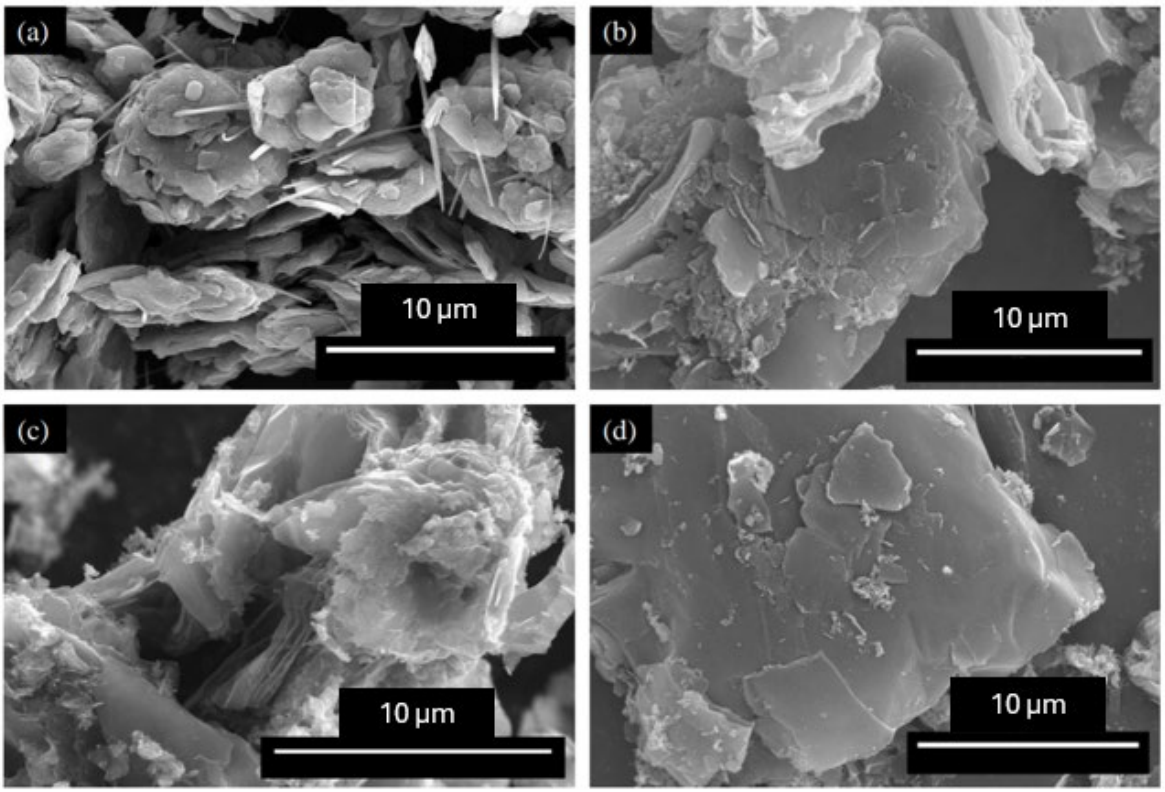

Figure 3: FESEM images of (a) rGO, (b) S-rGO, (c) N-rGO, and (d) F-rGO. All images are presented with consistent, clarified scale bars of 10 µm

Nitrogen-doped rGO (N-rGO, Figure 3(c)) shows a crumpled, fragmented morphology, indicating higher edge density and increased defect concentration. This is favorable for electrochemical activity due to enhanced electrolyte contact and ion diffusion. The EDX profile (Figure 4(b)) confirms nitrogen presence at 1.7 percent by weight and 1.4 percent by atomic content. Such crumpled and defect-rich morphology is consistent with previous findings, where nitrogen-doped reduced graphene oxide with higher edge-site density demonstrated enhanced electrolyte accessibility and improved lithium-ion diffusion kinetics as anode materials [6]. In contrast, fluorine-doped rGO (F-rGO, Figure 3 (d)) exhibits a more compact and smoother sheet morphology, indicating reduced defect density and more orderly stacking. The EDX data (Figure 4(c)) confirms the successful doping with fluorine, measured at 1.8

percent by weight and 1.2 percent by atomic percentage. Fluorine, being highly electronegative, tends to stabilize the graphene structure and can enhance its hydrophobicity and chemical resistance, which are beneficial for improving electrode durability under electrochemical cycling. Prior research confirmed that F-doping reduces structural disorder and enhances electrode stability under repeated cycling as found in previous work [9].

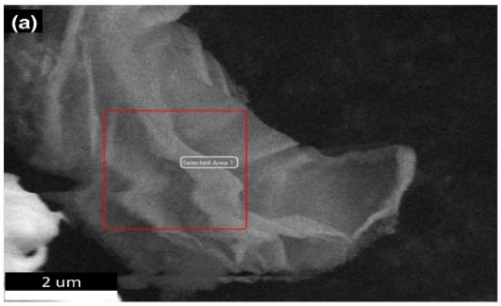

eZAF Quant Result - Analysis Uncertainty: 8.85 %

Element	Weight %	Atomic %
C	85.5	91.1
O	7.6	6.1
F	0.2	0.2
Al	0.2	0.1
S	6.4	2.6

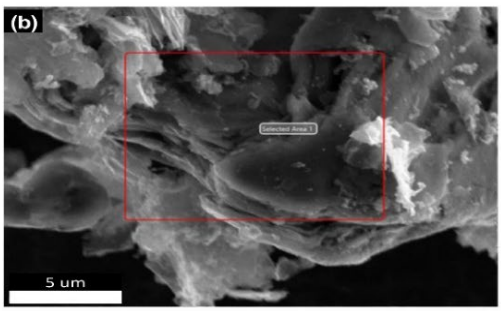

eZAF Quant Result - Analysis Uncertainty: 7.92 %

Element	Weight %	Atomic %
C	92.9	94.4
N	1.7	1.4
O	5.5	4.2

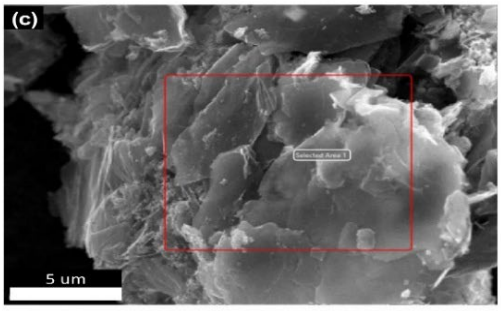

eZAF Quant Result - Analysis Uncertainty: 7.14 %

Element	Weight %	Atomic %
C	91.3	93.5
N	0.8	0.7
O	6.0	4.6
F	1.8	1.2

Figure 4: EDX spectra of functionalized rGO samples: (a) S-rGO, (b) N-rGO, and (c) F-rGO

The combined FESEM and EDX analyses confirm that the hydrothermal and thermal doping strategies effectively alter both the morphology and elemental composition of rGO. Sulfur and nitrogen doping introduce more defects and crumpled features favorable for high reactivity, whereas fluorine doping promotes planarization and structural integrity. These variations are crucial for tuning the electrochemical behavior of rGO-based anodes in lithium-ion battery applications.

3.2 Electrochemical Performance

Figure 5 shows the cyclic voltammetry (CV) profiles of pristine reduced graphene oxide (rGO) and its heteroatom-doped derivatives, including nitrogen-doped (N-rGO), fluorine-doped (F-rGO), and sulfur-doped (S-rGO). All electrodes were evaluated in a half-cell configuration using lithium metal as both the counter and reference electrode within a potential window of 0.01–3.0 V (vs. Li/Li^+). The CV curves exhibit pronounced differences in current response and enclosed area, reflecting variations in electrochemical activity and charge storage behavior induced by different heteroatom dopants. Notably, S-rGO displays a significantly larger CV-integrated area compared to the other samples, indicating an enhanced charge storage capability with substantial surface-controlled contributions. Based on quantitative analysis of the CV data, the apparent capacitance values were estimated to be 492.32 F g^{-1}

for S-rGO, 417.66 F g^{-1} for rGO, 278.39 F g^{-1} for N-rGO, and 223.07 F g^{-1} for F-rGO. Because standard lithium-ion battery performance is typically evaluated in terms of capacity, these apparent capacitance values were mathematically converted to CV-derived specific capacities using the formula Capacity = (C × ΔV) / 3.6, where ΔV is the operational voltage window (2.99 V). Consequently, the estimated specific capacities are 408.90 mAh g^{-1} for S-rGO, 346.89 mAh g^{-1} for rGO, 231.21 mAh g^{-1} for N-rGO, and 185.27 mAh g^{-1} for F-rGO. While future galvanostatic charge-discharge (GCD) testing will be required to comprehensively evaluate long-term cycling stability, these CV-derived capacities provide a standard comparative metric for battery applications.

The enhanced electrochemical performance of S-rGO is hypothesized to be associated with the incorporation of sulfur-containing functional groups, such as C–S–C and SO_x species, which potentially introduce electrochemically active defect sites. While the significantly enlarged CV-integrated area suggests possible surface-dominated Faradaic contributions, detailed kinetic analyses at multiple scan rates are required in future studies to definitively confirm the pseudocapacitive charge storage mechanisms. Interestingly, while sulfur doping reduces the interlayer d-spacing to 0.336 nm (compared to 0.365 nm for pristine rGO), it simultaneously yields the highest crystallinity (62 %). The enhanced electrochemical performance of S-rGO which yielding the highest apparent capacitance of 492.32 F g^{-1} (408.90 mAh g^{-1}) is therefore predominantly driven by its rich defect chemistry rather than expanded diffusion pathways. The abundant electrochemically active sulfur-containing functional groups (such as C–S–C and SO_x species) facilitate surface-dominated Faradaic reactions that overcome the reduced interlayer spacing, enhancing the overall pseudocapacitive charge storage behavior. These findings are in good agreement with previous studies reporting that sulfur-doped graphene-based materials exhibit superior charge storage characteristics owing to their rich defect chemistry, redox activity, and improved ionic transport pathways. Furthermore, recent studies have demonstrated that sulfur-enriched interphases and scaffolded architecture contribute to enhanced ionic transport and improved long-term electrochemical performance in lithium-based energy storage systems. This aligns with recent mechanistic insights by Song et al. [17] who demonstrated that sulfur-enriched interphases facilitate rapid ion transport; similarly, in our system, the incorporated sulfur species act as active defect sites that visibly accelerate interfacial kinetics, resulting in our highest observed apparent capacitance of 492.32 Fg^{-1}.

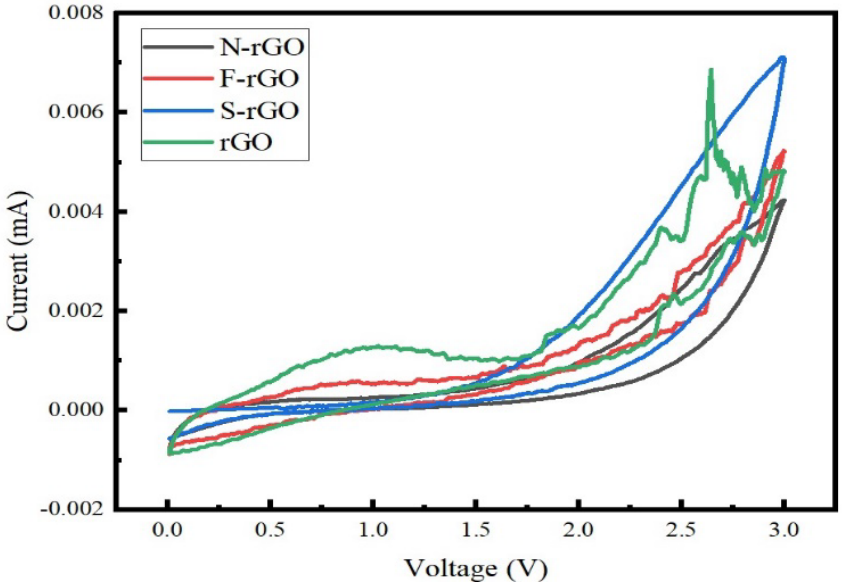

Figure 5: Cyclic voltammetry (CV) curves of rGO and heteroatom-doped rGO (N-rGO, F-rGO, S-rGO) anodes measured in half-cell configuration versus Li metal at a scan rate of 0.2 mV/s within the voltage window of 0.01–3.0 V (vs. Li/Li^+). All tested electrodes were formulated with a uniform active material mass loading of 1.0 mg cm^{-2} to ensure accurate and reliable cross-sample comparison

The undoped rGO sample also exhibited relatively high capacitance, which can be attributed to its large surface area, high electrical conductivity, and the presence of oxygen-containing groups that support electric double-layer capacitance. This result confirms the suitability of well-reduced graphene oxide as a base anode material for lithium-ion systems. In the case of N-rGO, the moderate CV-derived apparent capacitance indicates that while nitrogen doping can enhance electrical conductivity and introduce electrochemically active sites such as pyridinic and graphitic nitrogen, the overall electrochemical improvement is strongly dependent on the dopant configuration and concentration. Excessive defect formation or a reduction in accessible surface area resulting from inappropriate nitrogen incorporation may limit its contribution to surface-controlled charge storage behavior. For F-rGO, the lowest apparent capacitance of 223.07 F g^{-1} (185.27 mAh g^{-1}) quantitatively aligns with its structural consolidation. The reduction in the interlayer d-spacing to 0.337 nm, combined with a relatively low crystallinity of 47 %, physically restricts the ion accessibility within the layers. Furthermore, the formation of highly polar C–F bonds disrupt the delocalized π-electron system of graphene, leading to reduced electronic conductivity and hindered lithium-ion transport. Although fluorine doping can improve surface wettability and structural stability, it may simultaneously introduce unfavorable electronic and structural effects that suppress charge storage performance. This interpretation is consistent with recent findings by Das et al., [18] who demonstrated that highly polar catalytic interfaces drastically alter redox dynamics; in our case, the highly electronegative C–F bonds appear to restrict the desired surface-dominated charge storage, yielding the lowest capacitance of 223.07 F g^{-1}.

When compared to rGO–metal oxide composites, which often report higher apparent capacitance values (typically 500–700 F g^{-1}), largely arising from bulk redox processes, the doped-rGO materials offer several practical advantages [19]. Metal oxide-based composites derive their capacitance primarily from bulk redox reactions but often suffer from poor structural stability and capacity fading due to mechanical stress from volumetric expansion during cycling. Additionally, the synthesis of such composites is usually more complex and less environmentally sustainable. In contrast, heteroatom-doped rGO materials maintain excellent electrical conductivity and structural integrity, highlighting their potential as viable anode materials, though further long-term cycling studies are required to fully validate their performance. Their synthesis is relatively straight forward and can be achieved using simple thermal or hydrothermal treatments with dopant precursors such as urea, thiourea, or fluorinated salts. Furthermore, when benchmarked against recent state-of-the-art heteroatom-doped graphene and carbon-based anodes, which typically exhibit apparent capacitances in the range of 300 to 450 F g^{-1} depending on the dopant configuration [20], the optimized S-rGO synthesized in this study (492.32 F g^{-1}) demonstrates highly competitive electrochemical performance. This indicates that our simplified synthesis route successfully maximizes the active defect chemistry without requiring complex hybrid architectures. Overall, these findings demonstrate that heteroatom doping can significantly tailor the electrochemical behavior of graphene-based anode materials. Among the samples investigated, S-rGO displayed the most promising performance, followed by pristine rGO, N-rGO, and F-rGO. The results suggest that sulfur doping offers the most beneficial effect in enhancing surface-dominated charge storage behavior and lithium-ion storage, thereby supporting the potential of functionalized graphene materials as effective anodes for lithium iron phosphate battery systems. This agrees with insights from light-assisted and sulfur-anchoring strategies where dopant synergy and layered hybrid scaffolds lead to long-term stability and rate performance improvements [21].

4. CONCLUSIONS

Heteroatom doping has proven to be an effective strategy for enhancing the electrochemical performance of reduced graphene oxide as a potential anode material for lithium iron phosphate battery systems. Among the investigated samples, sulfur-doped rGO exhibited the most pronounced electrochemical response, as reflected by the largest CV-enclosed area, corresponding to the highest CV-derived apparent capacitance value of 492.32 F g^{-1}. Structural and morphological analyses revealed that sulfur and nitrogen dopants introduced increased surface roughness and defect density, which promoted electrochemically active sites and enhanced surface-controlled charge storage behavior. In

contrast, fluorine doping improved the compactness and structural stability of the graphene layers, albeit at the expense of reduced electrochemical activity. These variations in performance are closely correlated with the nature of the dopant and its influence on the electronic structure and defect chemistry of rGO. Compared to more complex metal oxide composites, heteroatom-doped rGO materials offer a structurally tailorable and environmentally benign approach while maintaining competitive initial electrochemical characteristics. While the current structural evaluations provide a robust macroscopic foundation, future studies will incorporate high-resolution transmission electron microscopy (HRTEM) to provide deeper atomic-level validation of the dopant-induced lattice structures and defect distributions. Furthermore, subsequent investigations will incorporate X-ray photoelectron spectroscopy (XPS) to definitively resolve the specific dopant bonding configurations (e.g., pyridinic-N, thiophene-S, and C–F bonds) and quantitatively link these distinct functional states to the fundamental charge storage kinetics. Also, future work will focus on extensive GCD, EIS, and long-term cycling stability tests in full-cell configurations. Overall, the findings provide a viable pathway for the development of high-performance, functionalized graphene-based anode materials that can address the growing demands for energy-dense, stable, and efficient lithium-ion battery technologies.

Acknowledgement

The authors express their gratitude to the Centre for Research and Innovation Management (CRIM), Universiti Teknikal Malaysia Melaka (UTeM), for their valuable support and fund in this research through the PJP Perintis Grant (PJP/2024/FTKE/PERINTIS/S01986). Furthermore, the authors would like to express their sincere appreciation to Prof. Noriyoshi Matsumi and Dr. Bharat Sri Mitra at the Japan Advanced Institute of Science and Technology (JAIST) for their invaluable supervision, technical support, and provision of the electrochemical laboratory facilities utilized to conduct the cyclic voltammetry (CV) testing.

Author Contributions

All authors contributed toward data analysis, drafting and critically revising the paper and agree to be accountable for all aspects of the work.

Disclosure of Conflicts of Interest

The authors have no disclosure to declare.

Compliance with Ethical Standards

The work adheres to ethical standards, ensuring that all experimental procedures and methodologies were conducted with integrity and respect for ethical guidelines.

References

[1] Manthiram, A. (2020). A reflection on lithium-ion battery cathode chemistry. *Nature Communications*, 11(1), 1550.

[2] Li, M., Lu, J., Chen, Z. & Amine, K. (2018). 30 years of lithium-ion batteries. *Advanced Materials*, 30(33), 1800561

[3] Zhu, L. W., Zhao, S., Lu, B., Jiang, F., Lu, Z. & Xu, Z. (2024) Structures, performances and applications of green biomass derived carbon in lithium-ion batteries. *Energy Materials,* 2024(4),400078

[4] K. K. R., Rajaji, U., Liu, T. Y., Kumar, V. (2025) Charge injection dynamics in oxygen-functionalized and heteroatom-doped reduced graphene oxide and their impact on supercapacitor performance: An experimental and DFT investigation. *Journal of Electroanalytical Chemistry*, 977(3), 118848.

[5] Yang, Z., Xu, Y., Sun, S., Zhang, Y., Li, X., Zhao, Y., Hao, X., Xue, C., Guo, D., Li, J. & Wang, J. (2025) Electrical energy storage from low-grade heat using reduced graphene oxide–carbon nanotube composite materials. *Materials,* 18(20), 4807.

[6] Tasdemir, A., Bulut Kopuklu, B., Kirlioglu, A. C., Alkan Gursel, S. & Yurum, A. (2021). The influence of nitrogen doping on reduced graphene oxide as highly cyclable Li-ion battery anode with enhanced performance. *International Journal of Hydrogen Energy*, 46(21), 11865–11877.

[7] Aslam, J. & Wang, Y. (2023). Metal oxide wrapped by reduced graphene oxide nanocomposites as anode materials for lithium-ion batteries. *Nanomaterials*, 13(2), 296.

[8] Liu, J., Wang, M., Wang, Q., Zhao, X., Song, Y., Zhao, T. & Sun, J. (2022). Sea urchin-like Si@MnO_2@rGO as anodes for high-performance lithium-ion batteries. *Nanomaterials*, 12(2), 285.

[9] Lee, Y.-K., Lee, C.-H., Kang, G.-S. & Eom, K. S. (2021). Understanding an exceptionally fast and stable Li-ion charging of highly fluorinated graphene with fine-controlled C–F configuration. *ACS Applied Materials & Interfaces*, 13(49), 58628–58636

[10] Wang, Y., Hu, M., Ai, D., Zhang, H., Huang, Z.-H., Lv, R. & Kang, F. (2019). Sulfur-doped reduced graphene oxide for enhanced sodium ion pseudocapacitance. *Nanomaterials*, 9(5), 752

[11] Li, H., Zhang, B., Wang, X., Zhang, J., An, T., Ding, Z., Yu, W. & Tong, H. (2019). Heterostructured SnO_2-SnS_2@C embedded in nitrogen-doped graphene as a robust anode material for lithium-ion batteries. *Frontiers in Chemistry*, 7, 339..

[12] Kim, C.-W., Kim, U.-S. & Kang, Y.-C. (2021). Characteristics and electrochemical performances of silicon/carbon nanofiber/graphene composite films as anode materials for binder-free lithium-ion batteries. *Scientific Reports*, 11(1), 1092.

[13] Sun, P., Zhang, M., Liu, Y., Zhao, J., Yang, J., Wang, Y., Wang, Y. & Zhang, Z. (2024). 1T–2H $MoSe_2$/N-doped rGO composites as anodes for high performance lithium-ion batteries. *New Journal of Chemistry*, 48(3), 1372–1380

[14] Huang, H.-H., De Silva, K. K. H., Kumara, G. R. A. & Yoshimura, M. (2018). Structural evolution of hydrothermally derived reduced graphene oxide. *Scientific Reports*, 8(1), 6849.

[15] Pal, N. & Bhattacharyya, A. J. (2023). Probing the 'universal' amorphization of crystalline sulfur in its mixture with ultrahigh surface area porous carbon. *The Journal of Physical Chemistry C*, 127(12), 5713–5719.

[16] dos Reis, G. S., Conrad, S., Lima, E, C., Naushad, M., Manavalan, G., Gentili, F. G., Dotto, G. L. & Grimm, A. (2024) Synthesis of highly porous lignin-sulfonate sulfur-doped carbon for efficient adsorption of sodium diclofenac and synthetic effluents. *Nanomaterials,* 15(24), 1860.

[17] Song, K. M., Chang, S. Y., Yuan, Y., Zeng, F., Li, N., Chen, H., Lu, P., Yuan, N. & Ding J. (2025). Constructing an organic–inorganic hybrid solid-electrolyte interface in situ via an organo-polysulfide electrolyte additive for lithium–sulfur batteries. *ACS Applied Materials & Interfaces*, 17(35), 8526–8536.

[18] Das, A. K., Yadav, P., Verma, T. S., Thripuranthaka, M., Krishnamurty, S. & Shelke, M. V. (2025). Unlocking enhanced redox dynamics: The power of a bifunctional catalytic zinc phosphide interface in full cell and pouch lithium–sulfur batteries. *ACS Applied Materials & Interfaces*, 17(5), 7657–7669

[19] Mummoorthi, G., Shajahan, S., Abu Haija, M., Mahalingam, U. & Rajendran, R. (2022) Synthesis and characterization of ternary α-Fe2O3/NiO/rGO composite for high-performance supercapacitors. *ACS Omega,* 7(31), 27390–27399.

[20] Kaur, A., Pandey, O. P. & Brar, L. K. (2026). Ternary heteroatom (B, P, N) doped graphene for high-performance supercapacitors. *RSC Advances,* 16(10), 8682–8692.

[21] Meng, T., Wang, X., Zhao, W., Gao, Y., Geng, Z., Chen, J., Bu, F., Zhu, H., Li, J., Zhang, H. & Guan, C. (2025). Coupling bifunctional scaffolds with slow photon effect for synergistically enhanced photoassisted lithium–sulfur battery properties. *ACS Nano*, 19(4), 4901–4912.